6th International Conference on Computational and Mathematical Biomedical Engineering – CMBE2019
10-12 June 2019, Japan
P. Nithiarasu, M. Ohta, M. Oshima (Eds.)

MODELLING THE DEFORMATION BEHAVIOR OF STOMATOCYTE, DISCOCYTE AND ECHINOCYTE RED BLOOD CELL MORPHOLOGIES DURING OPTICAL TWEEZERS STRETCHING

Nadeeshani Maheshika Geekiyanage[1], Emilie Sauret[1], Suvash Saha[2], Robert Flower[3], and YuanTong Gu[1]
[1] School of Chemistry, Physics and Mechanical Engineering, Queensland University of Technology (QUT), Brisbane, Queensland, Australia, emilie.sauret@qut.edu.au
[2] University of Technology Sydney (UTS), New South Wales, Australia
[3] Research and Development, Australian Red Cross Blood Service, Brisbane, Queensland, Australia

SUMMARY

A coarse-grained (CG) red blood cell (RBC) membrane model is used to investigate the deformation behavior of stomatocyte, discocyte and echinocyte morphologies during optical tweezers stretching. First, the numerically predicted discocyte deformation behavior is validated against analogous experimental observations, and then the numerically predicted stomatocyte and echinocyte deformation behavior is compared to the discocyte deformation behavior. The findings indicate that the CG-RBC membrane model is capable of accurately predicting the deformation behavior of stomatocyte, discocyte and echinocyte RBC morphologies during optical tweezers stretching, and an applicable tool to investigate the evolution of RBC behavior and membrane properties for different morphologies.

Key words: *Red Blood Cell, Optical Tweezers Stretching, Stomatocyte, Echinocyte*

1 INTRODUCTION

The RBC morphology affects its deformability, and optical tweezers stretching experiments can be used to investigate the global deformability of different RBC morphologies. Many optical tweezers stretching investigations have been conducted experimentally and numerically to study the discocyte RBC deformation behavior [1-3], but limited studies have been conducted on stomatocyte and echinocyte morphologies. Consequently, there is limited understanding of the influence of different RBC morphologies on its deformability and membrane mechanical properties. Improved understanding on above aspects during RBC morphology transformation can assist in identifying membrane structural modifications during in-vitro RBC storage and hematological disorders [4-6], which lead to RBC morphological changes and reduced deformability. In this study, a CG-RBC membrane model is proposed to investigate the global deformation behavior of different RBC morphologies.

2 METHODOLOGY

The coarse-grained RBC (CG-RBC) membrane model is built by a 2D triangulated network of N_v $(= 2{,}562)$ vertices having N_t $(= 5{,}120)$ triangular elements and N_s $(= 7{,}680)$ adjacent vertex-vertex connections. The triangulated network is composed of only 12 vertices (=0.47%) having 5 adjacent vertex-vertex connections, whereas all the remaining membrane vertices (=99.53%) have 6 adjacent vertex-vertex connections. Therefore, the CG-RBC membrane has high quality of triangulation, and the effects of inhomogeneity can be considered minimal. The RBC membrane free energy is the collective contribution of in-plane stretching energy ($E_{Stretching}$), out-of-plane bending energy

($E_{Bending}$), and constraints of reference cell surface area ($E_{Surface\ Area}$) and cell volume (E_{Volume}). $E_{Stretching}$ is estimated based on the coarse-graining approach implemented by Fedosov et al. [3], and is given by

$$E_{Stretching} = \sum_{j \in 1 \dots N_s} \left[\frac{k_B T l_{max} \left(3 x_j^2 - 2 x_j^3\right)}{4 p (1 - x_j)} + \frac{k_p}{(m-1) l_j^{m-1}} \right] \quad (1)$$

where, l_j is the length of j^{th} link, k_B is the Boltzmann constant, T ($= 296.15\ K$) is the absolute temperature, l_{max} is the maximum link extension, p is the persistence length, k_p is the power function coefficient, and m ($= 2$) is an exponent such that $m > 0$. x_j is defined as $x_j = l_j / l_{max}$. Following the CG-RBC membrane model [3], the membrane shear modulus [μ_0 ($= 4.0\ \mu N m^{-1}$)] [3, 6] can be expressed as:

$$\mu_0 = \frac{\sqrt{3}\, k_B T}{4 p\, l_{max}\, x_0} \left(\frac{x_0}{2 (1 - x_0)^3} - \frac{1}{4 (1 - x_0)^2} + \frac{1}{4} \right) + \frac{\sqrt{3}\, k_p\, (m+1)}{4\, l_0^{m+1}} \quad (2)$$

where, l_0 is the equilibrium length of spectrin link and defined as $x_0 = l_0 / l_{max}$ ($= 0.45$). The parameters k_p and p can be estimated for a given μ_0 and x_0 using Equation (1) and Equation (2) at the equilibrium state of specified cytoskeletal reference state.

$E_{Bending}$ is estimated based on a discrete approximation of the Helfrich energy model [7] for a zero spontaneous membrane curvature, and is given by

$$E_{Bending} = 2\, \kappa \sum_{j \in 1 \dots N_s} \frac{M_j^2}{\Delta A_j} \quad (3)$$

where κ ($= 2.5 \times 10^{-19}\ Nm$) [6, 8] is the bending modulus, M_j is the membrane curvature at the triangle-pair that shares the j^{th} link, and ΔA_j represents the surface area associated with the j^{th} link. M_j and ΔA_j are given by

$$M_j = \frac{1}{2}\, l_j\, \theta_j \quad (4)$$

$$\Delta A_j = \frac{1}{3} (A_{T1} + A_{T2}) \quad (5)$$

where θ_j is the angle between outward normal vectors to the triangles sharing j^{th} link, and A_{T1} and A_{T2} are the planer area of $T1$ and $T2$ triangles respectively that share the j^{th} link. $E_{Surface\ Area}$ and E_{Volume} are estimated according to Equation (6) and Equation (7) [3, 9], and the first part of Equation (6) represents the total surface area constraint whereas the second part represents the triangular element surface area constraint.

$$E_{Surface\ Area} = \frac{1}{2}\, k_A \left(\frac{A - A_0}{A_0} \right)^2 A_0 + \sum_{k \in 1 \dots N_t} \frac{1}{2}\, k_a \left(\frac{A_k - A_{k,0}}{A_{k,0}} \right)^2 A_{k,0} \quad (6)$$

$$E_{Volume} = \frac{1}{2}\, k_v \left(\frac{V - V_0}{V_0} \right)^2 V_0 \quad (7)$$

where, A_0 ($= 140.0\ \mu m^2$) is the reference membrane surface area [4, 5], A is the instantaneous membrane surface area, $A_{k,0}$ is the reference area of k^{th} triangle, A_k is the instantaneous area of k^{th} triangle, V_0 ($= 93.48\ \mu m^3$) is the reference cell volume [4, 5] and V is the instantaneous cell volume. k_A ($= 1.0 \times 10^{-3}\ Nm^{-1}$, k_a ($= 5.0 \times 10^{-5}\ Nm^{-1}$) and k_v ($= 100.0\ Nm^{-2}$) represent the total surface area, local surface area and volume constraint coefficients, respectively.

A bilayer-coupling model (BCM) based approach is used to obtain stomatocyte, discocyte and echinocyte morphologies, and contributes to the membrane energy through bilayer-leaflet-area-difference ($E_{Area-difference}$) and total-membrane-curvature constraints ($E_{Total-curvature}$). $E_{Area-difference}$ to maintain a reference bilayer-leaflet-area-difference (ΔA_0) is given by

$$E_{Area-difference} = \frac{1}{2} \frac{\pi\, k_{ad}}{D_o^2} \left(\frac{\Delta A - \Delta A_o}{A} \right)^2 A \quad (8)$$

where, k_{ad} ($= 300.0\ \kappa$) is the bilayer-leaflet-area-difference constraint coefficient, D_0 ($= 2.0\ nm$) is the monolayer thickness, and ΔA is the instantaneous bilayer-leaflet-area-difference which is estimates as follows.

$$\Delta A = 2\, D_0 \sum_{j \in 1 \dots N_s} M_j \quad (9)$$

$\Delta A_0 / A_0 (\%) = 0.105, 0.120$ and 0.190 for stomatocyte, discocyte and echinocyte morphologies, respectively. $E_{Total-curvature}$ to maintain a reference total-membrane-curvature (C_0) is given by

$$E_{Total-curvature} = \frac{1}{2}\frac{\pi k_C}{D_o^2}\left(\frac{C-C_o}{A}\right)^2 A \quad (10)$$

where $k_C\ (= 100.0\,\kappa)$ is the total-membrane-curvature constraint coefficient, and C is the instantaneous total-membrane-curvature which is estimated as follows.

$$C = 2\,D_o\,\sum_{j\,\in 1\ldots N_s}|M_j| \quad (21)$$

$C_0/A_0(\%) = 0.175, 0.185$ and 0.550 for stomatocyte, discocyte and echinocyte morphologies, respectively. Therefore, the total free energy (E) of the RBC membrane is given by

$$E = E_{Stretching} + E_{Bending} + E_{Surface\,Area} + E_{Volume} + E_{Area-difference} + E_{Total-curvature} \quad (12)$$

The optical tweezers stretching forces from $0 - 200\,pN$ is applied to the opposite ends of the cell [2, 3] along the principle axis of inertia through silica beads of $4.2\,\mu m$ in diameter at $2.0\,\mu m$ contact diameter, and stretched. The methodology of optical tweezers stretching implementation is adopted from Fedosov et al. [3], and the stable equilibrium RBC configuration is obtained at the minimum membrane free energy configuration under the externally applied stretching forces.

3 RESULTS AND CONCLUSIONS

The global cell deformability is numerically investigated for stomatocyte, discocyte and echinocyte morphologies through optical tweezers stretching deformation. Figure 1 presents the RBC membrane vertex points subjected to stretching force through attached silica beads of same size and at equal contact diameter. The contact area between RBC membrane and silica beads is similar for the stomatocyte and discocyte morphologies, whereas it is lower for the echinocyte. The spicules on the echinocyte cell surface reduce the contact between RBC membrane and beads, resulting in lower contact area.

Figure 1: Optical tweezers stretching implementation on (a) stomatocyte, (b) discocyte and (c) echinocyte morphologies

The variation of axial (D_A) and transverse (D_T) cell diameters [2, 3] at equilibrium is monitored at stretching forces analogous to optical tweezers stretching experiments by Suresh et al. [1]. The equilibrium stomatocyte, discocyte and echinocyte cell morphologies at $100\,pN$ stretching force are presented in Figure 2. The stomatocyte and echinocyte morphologies have conserved their morphology characteristics during optical tweezers stretching, though the biconcave discocyte shape has lost its biconcavity. Figure 3 presents the percentage change in D_A and D_T cell diameters for stomatocyte and discocyte at similar μ_0 and κ [10], along with analogous experimental observations by Suresh et al. [1]. The discocyte stretching response agrees with experimental observations, and has a maximum deviation of ~ 10.0 % with respect to analogous experimental stretching, whereas the stomatocyte stretching response indicates higher global deformability than the discocyte. The echinocyte morphology shows the experimentally observed stiffer nature [11] at a membrane shear modulus above $2.5\mu_0$, which is comparable to experimental estimations [12].

Figure 2: Morphology deformation of (a) stomatocyte, (b) discocyte and (c) echinocyte RBCs under $40\,pN$ optical tweezers stretching force

In conclusion, the study investigates the deformation behavior of stomatocyte, discocyte and echinocyte morphologies under optical tweezers stretching, using a coarse-grained red blood cell membrane model that agrees well with analogous experimental observations. Therefore, the current

model is an applicable tool to further investigate the evolution of RBC behavior and membrane properties for different morphologies.

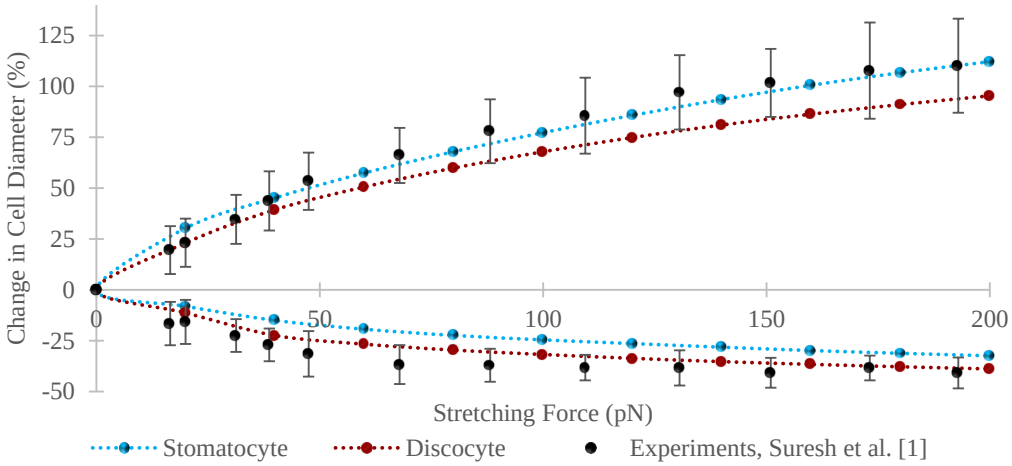

Figure 3. Numerically predicted change in D_A and D_T cell diameters for stomatocyte and discocyte morphologies at similar μ_0 and κ versus experimentally observed change in D_A and D_T for discocyte morphology by Suresh et al. [1]

REFERENCES

[1] S. Suresh *et al.*, "Connections between single-cell biomechanics and human disease states: gastrointestinal cancer and malaria," *Acta Biomaterialia,* vol. 1, no. 1, pp. 15-30, 2005.

[2] M. Dao, J. Li, and S. Suresh, "Molecularly based analysis of deformation of spectrin network and human erythrocyte," *Materials Science and Engineering: C,* vol. 26, no. 8, pp. 1232-1244, 2006.

[3] D. A. Fedosov, B. Caswell, and G. E. Karniadakis, "Systematic coarse-graining of spectrin-level red blood cell models," *Computer Methods in Applied Mechanics and Engineering,* vol. 199, no. 29–32, pp. 1937-1948, 2010.

[4] N. Mohandas and P. G. Gallagher, "Red cell membrane: past, present, and future," *Blood,* vol. 112, no. 10, pp. 3939-3948, 2008.

[5] G. Tomaiuolo, "Biomechanical properties of red blood cells in health and disease towards microfluidics," *Biomicrofluidics,* vol. 8, no. 5, p. 051501, 2014.

[6] X. Li, H. Li, H.-Y. Chang, G. Lykotrafitis, and G. E. Karniadakis, "Computational Biomechanics of Human Red Blood Cells in Hematological Disorders," *Journal of Biomechanical Engineering,* vol. 139, no. 2, pp. 021008-1-021008-13, 2017.

[7] K.-i. Tsubota, "Short note on the bending models for a membrane in capsule mechanics: Comparison between continuum and discrete models," *Journal of Computational Physics,* vol. 277, pp. 320-328, 2014.

[8] D. A. Fedosov, B. Caswell, and G. E. Karniadakis, "Coarse-Grained Red Blood Cell Model with Accurate Mechanical Properties, Rheology and Dynamics," in *Annual International Conference of the IEEE Engineering in Medicine and Biology Society*, vol. 1-20, 2009, pp. 4266-4269.

[9] M. Nakamura, S. Bessho, and S. Wada, "Analysis of red blood cell deformation under fast shear flow for better estimation of hemolysis," *International Journal for Numerical Methods in Biomedical Engineering,* vol. 30, no. 1, pp. 42-54, 2014.

[10] C. Monzel and K. Sengupta, "Measuring shape fluctuations in biological membranes," (in English), *Journal of Physics D-Applied Physics,* Review vol. 49, no. 24, p. 21, 2016, Art. no. 243002.

[11] Y. Park *et al.*, "Measurement of red blood cell mechanics during morphological changes," *Proceedings of the National Academy of Sciences of the United States of America,* vol. 107, no. 15, pp. 6731-6736, 2010.

[12] E. Kozlova, A. Chernysh, V. Moroz, V. Sergunova, O. Gudkova, and E. Manchenko, "Morphology, membrane nanostructure and stiffness for quality assessment of packed red blood cells," *Scientific Reports,* vol. 7, no. 1, p. 7846, 2017.